PROCEEDINGS OF SCIENCE

Progenitor constraint using line ratios of the CNO elements in supernova remnants

Hiroyuki Uchida[a,*] **and Takuto Narita**[a]

[a] *Kyoto University,*
Kitashirakawa Oiwake-cho, Sakyo, Kyoto, 606-8502, Japan

E-mail: uchida@cr.scphys.kyoto-u.ac.jp

Investigating the nature of progenitors is crucial for understanding the origin and mechanism of core-collapse and thermonuclear supernovae (SNe). While several methods have been developed to derive progenitor properties so far, many questions remain poorly understood. In this paper we demonstrate an observational approach to constrain progenitors of supernova remnants (SNRs) using abundances of carbon (C), nitrogen (N), and oxygen (O) in shock-heated circumstellar material (CSM). Our calculations with stellar evolution codes indicate that a total amount of these CNO elements will provide a more sensitive determination of the progenitor masses than the conventional method based on ejecta abundances. If the CNO lines (particularly those of C and N) are detected and measured their abundance ratios accurately, they can provide relatively robust constraint on the progenitor mass (and in some cases the rotation velocity) of SNRs. Since our method requires a better energy resolution and larger effective area in the soft X-ray band (< 1 keV), XRISM launched on September 7, 2023 and next-generation microcalorimeter missions such as Athena, Lynx, LEM, and HUBS will be adequate and will bring a new insight into link between the progenitors and their remnants.

Multifrequency Behaviour of High Energy Cosmic Sources XIV (MULTIF2023)
12-17 June 2023
Palermo, Italy

*Speaker

PoS(MULTIF2023)044

1. Introduction

While increasing diversity of supernova (SN) Types and subclasses has been reported so far, their progenitor origins and explosion mechanisms are still far from being well understood. Recent theories and observations indicate that their circumstellar environments are the key to understanding such a variety of spectra and light curves. It has been considered that several types of core-collapse (CC) SNe (e.g., Type IIn) can be related to a shock-heated circumstellar material (CSM) due to a high mass-loss rate [e.g., 1]; also, it has been recently realized that even in a regular Type II SN progenitors are commonly surrounded by the CSM that was evacuated just before the explosion [2]. Even in the case of Type Ia SNe, their circumstellar environments provide a clue to their origin since some of subclasses suggest massive CSM [e.g., 3] and more generally a low-density cavity might be formed by a mass-accreting white dwarf before the explosion [4, 5]. Therefore, observations of CSM around SNe are the key to understanding the explosion mechanisms of both CC and Type Ia SNe.

One of the most important topics in CC SNe is the progenitor mass distribution. Several observations of extra-galactic SNe provide a rough estimation of the mass range for explosion [e.g., 6, 7]. Recent observations of supernova remnants (SNRs) indicate that the ejecta abundance ratio of iron (Fe) to silicon (Si) shows a negative dependence on the zero-age main-sequence masses ($M_{\rm ZAMS}$) [8, 9] and they categorized progenitor masses of SNRs into three cases: 15 $M_\odot$ < $M_{\rm ZAMS}$, 15 $M_\odot$ < $M_{\rm ZAMS}$ < 22.5 $M_\odot$, and 22.5 $M_\odot$ < $M_{\rm ZAMS}$. While these studies are important for constraining $M_{\rm ZAMS}$ that can explode as SNe, it is required a more precise measurement of the lower/upper limits of $M_{\rm ZAMS}$. In this context, elemental abundances of shock-heated CSM in SNRs will provide rich information on progenitor parameters: $M_{\rm ZAMS}$, an initial rotation velocity, convection, etc. [e.g, 10–12]. This is also true in the case of Type Ia SNe, because part of Type Ia SNRs such as Kepler's SNR and N103B indicate strong evidence for shock-CSM interactions [13–16]. The presence of the CSM may hint at the origin of the Type Ia SN explosion, for which two scenarios are under debate: the double-degenerate [DD; 17, 18] or single-degenerate [SD; 19]. For instance, as previous studies indicate [e.g., 20], the presence of the nitrogen-rich CSM in Kepler's SNR support the SD scenario for the explosion. If this is the case, it may be possible to investigate the properties of a companion star, even though there is no promising candidate for a surviving star.

Since stellar winds contain material processed by the CNO cycle in stellar interiors, light elements such as carbon (C), nitrogen (N), and oxygen (O) most likely reflects the progenitor (or a companion star's) properties. It has been however difficult to detect the emission lines of especially C and N in shock-heated swept-up CSM with currently available X-ray detectors. This is mainly due to the lack of the energy resolution and effective area in the soft X-ray band, where the fluorescence lines of N VI Lyα (0.50 keV) and C V Lyα are expected. While several observations report detections of C and N lines in SNRs with CCDs [e.g., 21], they can be more clearly resolved with X-ray grating spectrometers, which have much better energy resolution [22].

We recently observed a magnetar-hosting SNR RCW 103 with the Reflection Grating Spectrometer (RGS) on board XMM-Newton and measured the N abundance of the CSM in this remnant for the first time [23]. By comparing the result with stellar evolution models, we successfully constrained $M_{\rm ZAMS}$ and initial rotation velocity of the progenitor of RCW 103 to be 10–12 $M_\odot$ and $\lesssim$ 100 km/s, respectively. The method presented here will be useful with upcoming X-ray

microcalorimeter observations with XRISM [24] launched in 2023 and future missions such as Athena [25], Lynx [26], LEM [27], and HUBS [28]. We thus demonstrate our calculation and method in this paper for near future high-energy-resolution X-ray observations of SNRs.

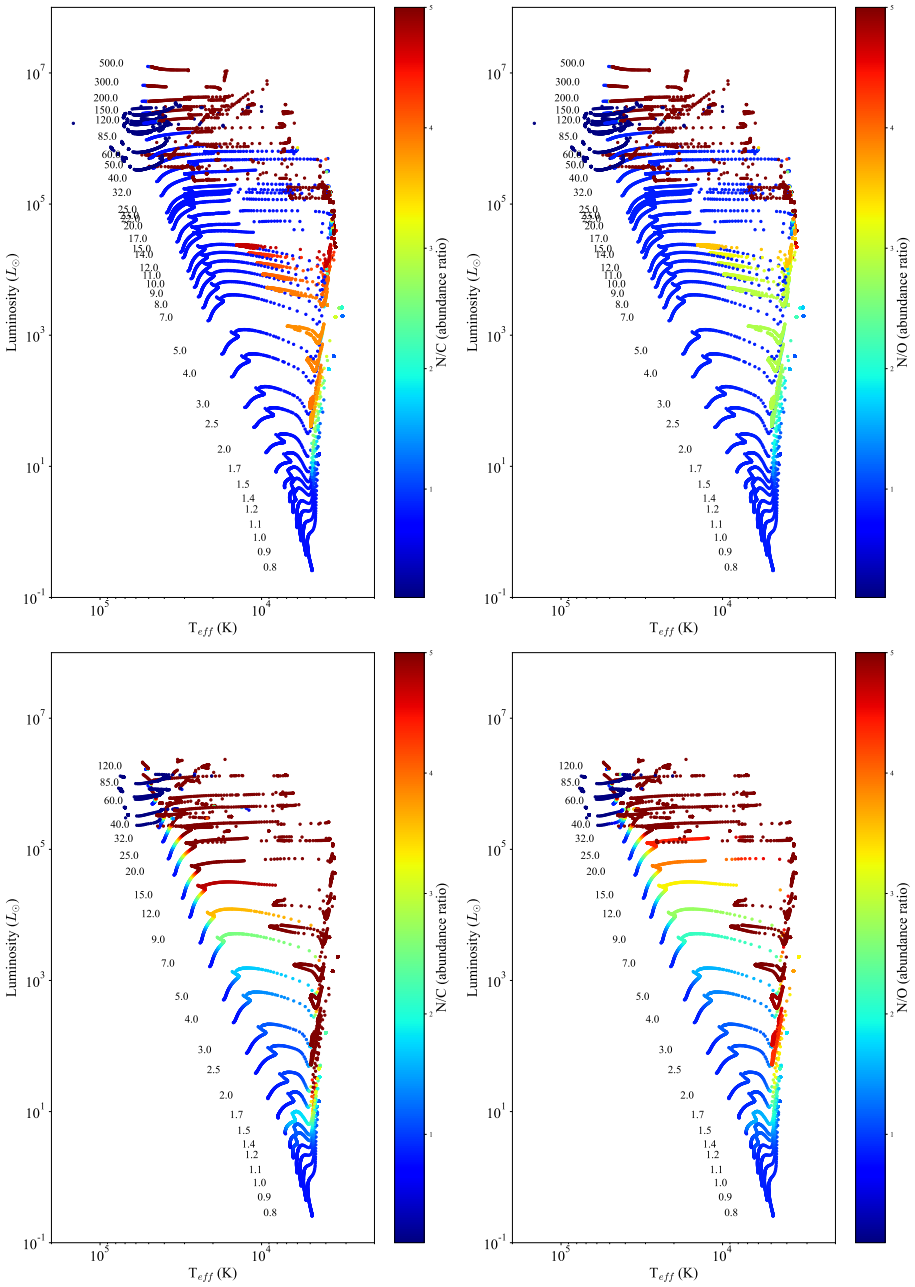

Figure 1: Hertzsprung–Russell diagram and calculated abundance ratios for various stars with different M_{ZAMS}, which are displayed at each start point of the main sequence. The color represents the abundance ratios of N/C (left) and N/O (right) that defined in equation 1.

2. Simulations and Calculations

To calculate expected abundance ratios for each progenitor mass, we used two stellar evolution codes: *HOngo Stellar Hydrodynamics Investigator, HOSHI* [29–32] and *Geneva* [33]. Here we focus on total yields of light elements that produced by the CNO cycle in the stellar interiors during their evolution. Since observationally it is useful to represent results in the form of so-called "solar abundance ratio", we define parameters as follows:

$$\mathrm{N/O} \equiv \frac{(n_\mathrm{N}/n_\mathrm{H})/(n_\mathrm{N}/n_\mathrm{H})_\odot}{(n_\mathrm{O}/n_\mathrm{H})/(n_\mathrm{O}/n_\mathrm{H})_\odot} = \frac{(n_\mathrm{N}/n_\mathrm{O})}{(n_\mathrm{N}/n_\mathrm{O})_\odot}, \tag{1}$$

where n_N, n_O, and n_H represent the number density of each element, and $(n_\mathrm{O}/n_\mathrm{H})_\odot$ means the solar abundance ratio [cf. 34]. Note that we show only the case of solar metallicity for the following calculations. This is because although total yields of the CNO elements highly depend on the stellar metallicity, their abundance ratios were almost unchanged and thus the following discussion is not significantly altered.

Figure 1 displays the Hertzsprung–Russell diagram and calculated abundance ratios of the CNO elements, which are produced inner layers and transferred to the stellar surface during each evolution stage with M_ZAMS. In every case, the abundance ratios are almost constant during the main sequence (MS) whereas they are increasing since N is accumulated at the post MS phase. The result is reasonably consistent with the standard picture of the massive star evolution. As also shown in the lower panels of Figure 1, we changed the initial rotation velocity $v_{init}/v_\mathrm{K} = 0.0$ to 0.3, where v_K is the Kepler velocity at the surface. As a result, in such fast-rotating star N is effectively evacuated and the resultant abundance ratios become larger. Additionally it is also effective in some cases that the centrifugal force efficiently promotes the convection and nuclear reactions though this effect is relatively negligible.

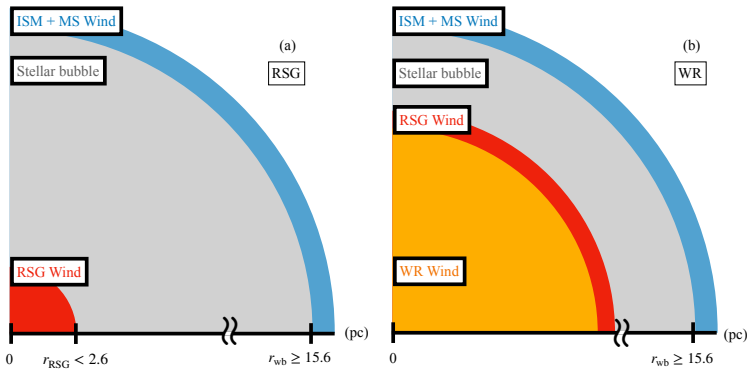

Figure 2: Schematic view of an environment around a star at the end of its life. *Left (a)*: Case of a low-mass star ending up as an RSG. Colors correspond to the shell of ISM and MS winds (blue), stellar bubble (grey), and RSG winds (red). *Right (b)*: Case of a high-mass star ending its life as a WR. The region dominated by a WR wind is represented as orange.

The elements transferred to the stellar surface (Figure 1) are mostly ejected by the stellar wind during each evolution phase. Total amounts of the CNO elements in the CSM are therefore time-integrated values and determined by mass-loss history of MS, red supergiant (RSG), and in some

cases Wolf-Rayet (WR) winds [35–37]. If we consider the abundance of shock-heated (swept-up) CSM for comparison with observations, the radial structure of their wind bubbles is also needed. We thus assume a simple geometrical configuration as illustrated in Figure 2. For example, the total MS wind mass depends on the progenitor $M_{\rm ZAMS}$, which can be calculated with the HOSHI code. The wind bubble size $r_{\rm wb}$ is typically calculated as

$$r_{\rm wb} = 15.6 \left(\frac{M_{\rm w}}{9.5 \times 10^{-1}\ M_\odot} \right)^{1/3} \left(\frac{v_{\rm w}}{10^3\ {\rm km\ s^{-1}}} \right)^{2/3}\ {\rm pc}, \tag{2}$$

where $M_{\rm w}$ and $v_{\rm w}$ are the total mass and velocity of the MS wind, respectively (for more details, see [23]). In the same manner, the size of the RSG wind $r_{\rm RSG}$ is estimated to be

$$r_{\rm RSG} \leq\ 2.6 \left(\frac{\dot{M}_{\rm w}}{5 \times 10^{-7}\ M_\odot\ {\rm yr^{-1}}} \right)^{1/2} \left(\frac{v_{\rm w}}{15\ {\rm km\ s^{-1}}} \right)^{1/2}\ {\rm pc}. \tag{3}$$

In the case of high-mass stars, a WR wind expands into the RSG-wind materials with a velocity of 100–200 km s^{-1} [37] during a WR phase duration of $\sim 10^{3\text{–}4}$ year for $M_{\rm ZAMS} \lesssim 60\ M_\odot$. Taking into account these properties, we illustrate a typical schematic view of a pre-SN environment in Figure 2. Since abundances of the CSM depend on where the SNR forward shock reached in the bubble, we consider three cases with different SNR radii $R_{\rm SNR}$, 1 pc, 5 pc, and 10 pc for the following calculations.

3. Results

Figure 3 shows calculated abundance ratios of N/C and N/O assuming the three cases with different radii explained above. We also calculated those for lower mass stars that do not explode as CC SNe as displayed in Figure 4. Note that the same plots of "mass ratios" as the x-axis are also given in Figures 6 and 7 in Appendix for convenience. MS stars emit a hydrogen(H)-rich wind whereas post-MS stars emit a stellar wind rich in helium (He) and N due to the convection, which carries the N-rich material from the the H-burning layer to the stellar surface [e.g, 38, 39]. In general, the total amount of ejected N positively correlated to $M_{\rm ZAMS}$ since the mass-loss rate has a positive relationship with the stellar mass [e.g., 40]. Therefore, an increasing trend of N/C and N/O can be clearly seen for lower-mass stars that end their lives as red giant (RG) stars ($\lesssim 3M_\odot$; Figure 4). A similar trend is also roughly seen in the case of $\gtrsim 20M_\odot$, $v_{init}/v_{\rm K} = 0.0$ (Figure 3). On the other hand, if the mass-loss rate is extremely high in a higher mass star, the N-rich wind is blown out in an earlier stage of evolution because of a stronger radiative force, so that N-rich CSM may be relatively far away from the progenitor; the inner C- and O-rich layer is emitted afterward. In this case, the resultant abundance ratios of N/C and N/O become lower. The entire trend therefore appears more complicated.

Another effect that changes the abundance ratios is especially considerable for lower-mass stars. Stars with $M_{\rm ZAMS} \simeq$ 4–8$M_\odot$ end up as an asymptotic giant (AGB) branch [e.g., 41], which results in a rapid increase of N at the early stage of the post MS phase: N-rich materials in the H-burning layer are carried to near the stellar surface by the so-called dredge-up [42]. As a result, most of the stellar wind material is ejected from the single N-rich layer regardless of $M_{\rm ZAMS}$, which leads to the almost constant trend in N/O. In the case of stars with $M_{\rm ZAMS}$= 10–12$M_\odot$, N-rich materials are

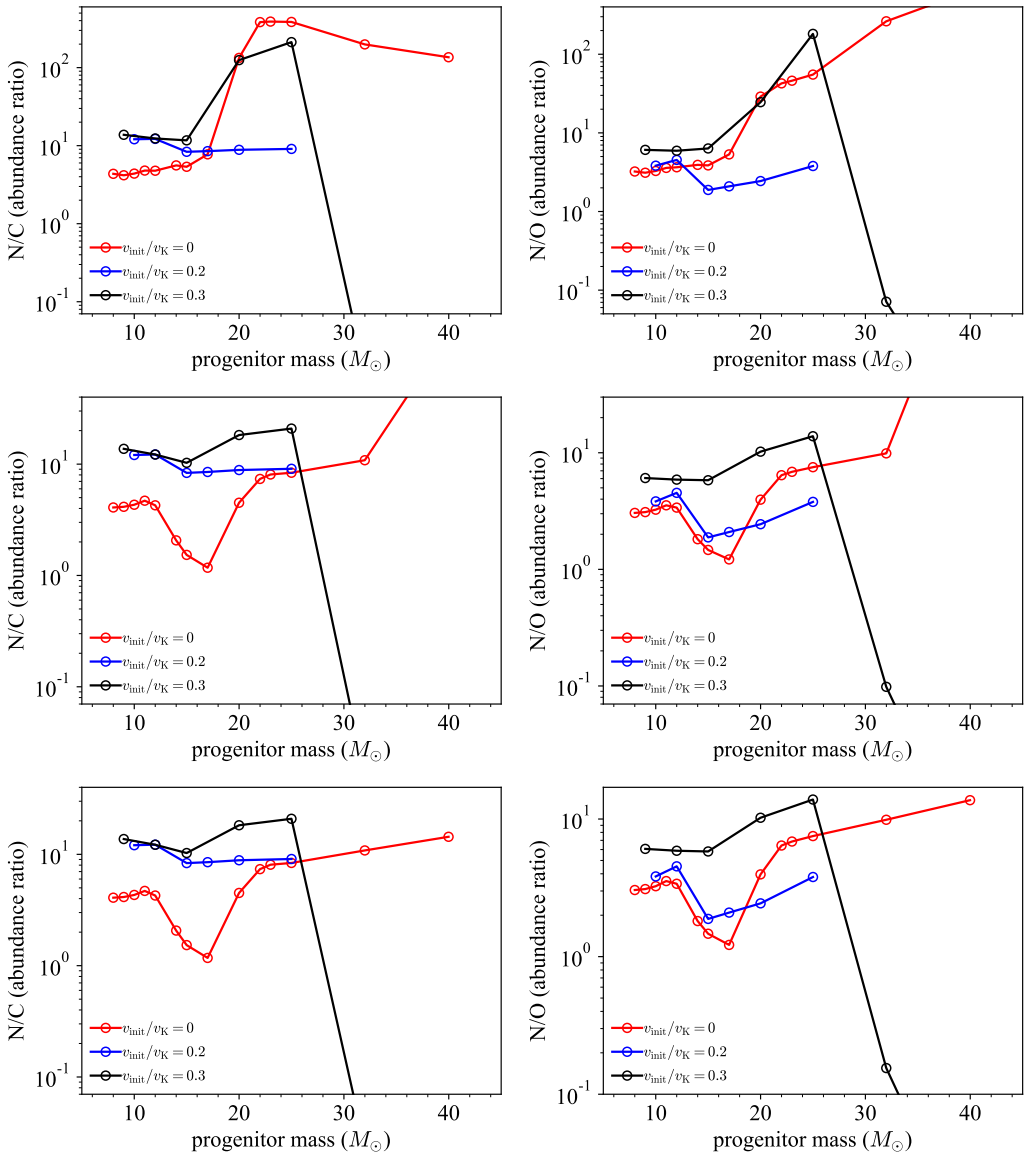

Figure 3: Abundances ratios (see equation 1) of N/C (the left panels) and N/O (the right panels) expected in the swept-up CSM with different $M_{\rm ZAMS}$ calculated with HOSHI and Geneva codes. The red, blue, and black circles correspond to cases of $v_{init}/v_{\rm K}$ = 0.0, 0.2, and 0.3, respectively. The top, middle, and bottom panels indicate that the shell size of the remnant is assumed to be 1 pc, 5 pc, and 10 pc in radius, respectively.

carried to the surface by convection; in some cases the He-burning occurs before the RSG phase, which prevents the star's expansion and hence an inefficient transfer of N.

The rotation velocity is also a considerable parameter; a faster rotation results in a more rapid increase of N during the stellar evolution. This is because the centrifugal force enhances the mass-loss rate at the stage of OB stars [38]. Note that additional N production by the CNO cycle is also enhanced in the post MS phase [43], which is however less effective. The effect of the stellar rotation can be typically seen in the cases of $M_{\rm ZAMS} \lesssim 20 M_\odot$ in Figures 3 and 4.

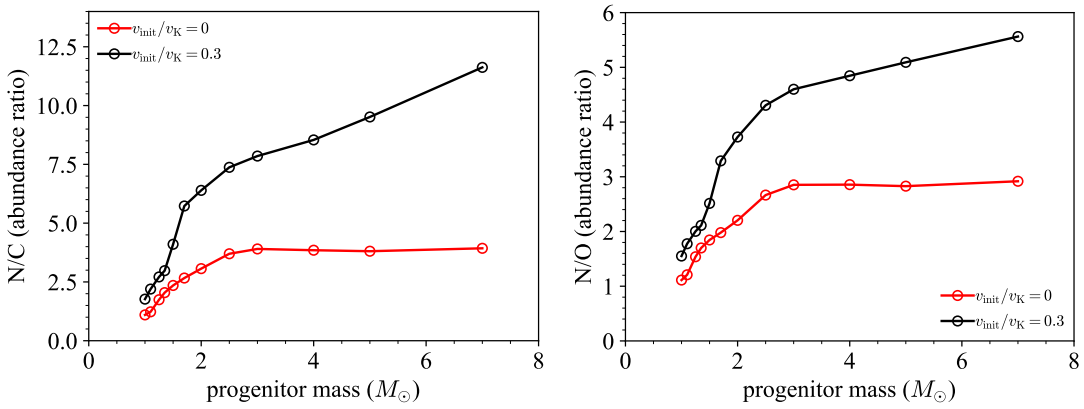

Figure 4: Same as Figure 3, but for lower-mass stars. The red and black circles correspond to cases of $v_{init}/v_{\rm K}$ = 0.0 and 0.3, respectively.

4. Discussion

4.1 Core-collapse SNRs

If the CNO lines are detected in an SNR and their abundances are measured, the plots shown in Figure 3 may be a good tool for estimating the progenitor properties of CC SNe more accurately than before, as is demonstrated by our previous work [23]. The most general method for this purpose is comparing an abundance ratio of (heavy) elements in ejecta with theoretically expected yield of explosive nucleosynthesis products. Recent study [9] however points out that this conventional method suffers a large uncertainty except for the Fe/Si ratio, which is relatively sensitive to progenitor core masses. Since all such methods using the ejecta abundance highly depend on supernova explosion theory, which is currently under progress, the mass estimation accuracy is less precise and provide a less stringent constraint on other parameters such as the rotation velocity. In contrast, the drawback of our method is the difficulty in detection of the CNO lines with currently available detectors, which should be overcome with future mission with a higher energy resolution and a larger effective area in the soft X-ray band (< 0.7 keV).

Figure 5 displays a N/C–N/O diagram based on our results shown in Figure 3. A clear correlation is found between the CNO abundances and the progenitor $M_{\rm ZAMS}$. It seems therefore promising to constrain $M_{\rm ZAMS}$ of SNRs by measuring both of N/C and N/O from a CSM spectrum, while C V Lyα (0.37 keV) is hard to detect in SNRs except for several examples [22]. If a systematic spectroscopy of SNRs is performed with a microcalorimeter such as *Resolve* onboard XRISM, its scattering plot will provide a clue to the progenitor mass distribution, which is observationally less understood [e.g., 44]. A caveat of using this method is that a uniform ambient density is tacitly assumed for calculating the size of the wind bubble; if an SNR is strongly interacting with dense clouds, it makes a larger uncertainty in the abundance estimates. Even if it were, this method will be still useful to estimate progenitor properties.

If the progenitor is in a binary system before its explosion, expected CNO abundance can be significantly changed and therefore our method cannot be used directly. In this case we can first

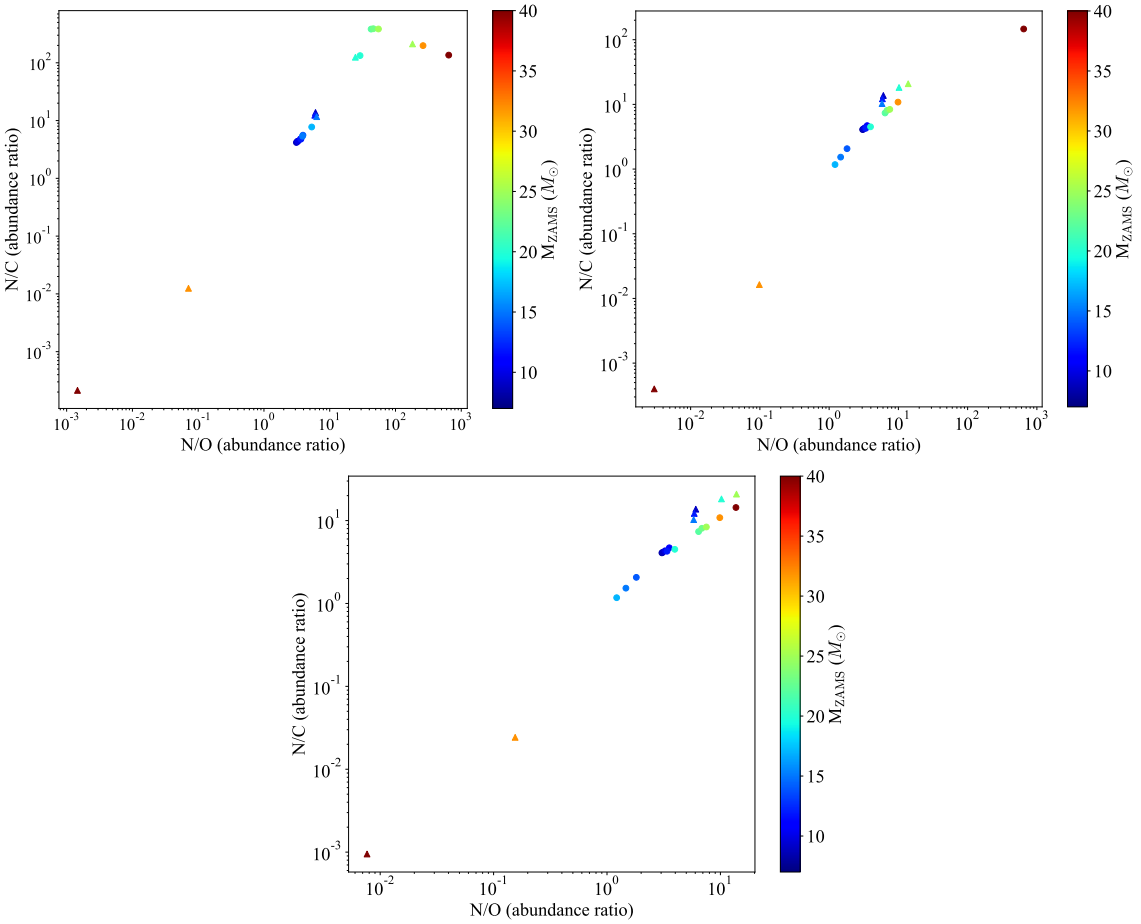

Figure 5: N/C versus N/O abundance ratios. The colored points indicate ratios obtained in our calculations. The circles and triangles represent cases of v_{init}/v_K = 0.0 and 0.3, respectively. The top left, top right, and bottom panels indicate that the shell size of the remnant is assumed to be 1 pc, 5 pc, and 10 pc in radius, respectively.

safely assume that the star experience a much stronger mass loss than that of a single star. Since inner H/He-burning layers tends to be exposed more effectively [e.g., 1], the progenitor star will end up as a WR star rather than a RSG star by enhanced mass stripping [45, 46]. We predict that such mass stripping results in a relatively low N/O in the CSM because O-rich material is blown off from the exposed surface by a WR wind. While it is generally hard to make a qualitative constraint and required an elaborate stellar wind simulation, one can roughly estimate the total amount of stripped envelope from the observed N/O. By comparing the result with binary evolution simulations, the progenitor (and companion star's) mass is roughly determined. A more detailed discussion will be given in our next paper [47], in which we found evidence for the binary remnant in a Galactic SNR.

4.2 Type Ia SNRs

Several observations of Type Ia SNRs suggest the presence of shock-heated dense gas, which is thought to be the CSM or a wind bubble created by an accreting progenitor white dwarf [e.g.,

Table 1: SNRs, in which abundances of the CNO elements were measured by previous studies so far.

Name	Age	C	N	O	N/O	ref.
	(yr)	(solar abundance)				
Galactic SNRs:						
Kepler's SNR	4×10^2	(=O)	$3.3^{+0.2}_{-0.3}$	1 (fixed)	$3.3^{+0.2}_{-0.3}$	[13]
RCW 103	2×10^3	(=O)	1.5 ± 0.1	$0.42^{+0.03}_{-0.01}$	3.8 ± 0.1	[23]
G296.1−0.5	2×10^4	(=O)	0.63 ± 0.07	0.17 ± 0.02	~ 3.7	[49]
Cygnus Loop	$(1–2)\times10^4$	0.20 ± 0.02	$0.26^{+0.18}_{-0.02}$	$0.18^{+0.02}_{-0.01}$	~ 1.4	[22]
SMC/LMC SNRs:						
SN 1987A	4×10	0.12	$1.05^{+0.16}_{-0.15}$	0.13 ± 0.02	~ 8.1	[50, 51]
N132D	2.5×10^3	$0.26^{+0.02}_{-0.01}$	$0.172^{+0.009}_{-0.001}$	$0.34^{+0.01}_{-0.02}$	~ 0.5	[52]
DEM L71	7×10^3	2.3 ± 0.8	0.35 ± 0.21	1 (fixed)	0.35 ± 0.21	[53]
N23	8×10^3	0.18 ± 0.03	0.07 ± 0.02	0.26 ± 0.01	~ 0.3	[54]
J0453.6−6829	$(1.2–1.5)\times10^4$	(=O)	1.5 ± 0.1	$0.42^{+0.03}_{-0.01}$	~ 0.7	[55]

13, 48]. As indicated in Figure 4, the result shows a monotonous increase in the amount of N with increasing $M_{\rm ZAMS}$. These ratios are thus also potentially useful for investigating the progenitor parameters of a companion star in a binary system, and are particularly important in the context of the origin of Type Ia SNe. Notably all the results significantly exceed the solar abundances; these ratios thus probe whether a forward-shock heated plasma is the CSM origin or interstellar matter (ISM) origin, which can be a good indicator for distinguishing between SD and DD progenitor scenarios. We note that in our calculation total amount of the ejected CNO elements is integrated from the MS to the final stage (e.g., RG or AGB) of stellar evolution. Although a mass-accreting wind expected for the SD system [4] makes the situation more difficult than the case of CC SNe, it is possible for our method to change the integration time in the same manner shown in [23], which may enable us to estimate plausible channels of the binary system such as WD/MS or WD/RG in a future analysis.

4.3 Current Observations and Future Prospects

Due to the lack of the energy resolution and the effective area of current X-ray detectors, samples that can be detected the CNO (especially C and N) lines are limited to those of less absorbed targets such as nearby or high galactic latitude SNRs. Table 1 shows a (not exhaustive) list of SNRs, in which the CNO abundances were measured with grating spectrometers so far. We found that all the Galactic SNRs have a high abundance ratio of N/O: at least two samples, RCW 103 and Kepler's SNR, are previously reported of a possible CSM interaction [14, 56]. Interestingly, SNRs in the large/small Magellanic clouds (LMC/SMC) listed in Table 1 have significantly lower N/O than the solar abundance ratio except for SN 1987A. The extremely high N/O found in SN 1987A is not surprising because there are many pieces of evidence for a shock-heated stellar wind material blown from the progenitor's RSG phase and the subsequent blue supergiant phases [57, 58]. In such case, the N-rich wind blown just before the SN explosion is dominant in the swept-up shock-heated

CSM, which gives a higher N/O. On the other hand, much lower N/O found in the other LMC/SMC SNRs would be notable. It cannot be explained by our model displayed in Figure 3. Although a more massive star case ($M_{\rm ZAMS}$ of $\gtrsim 30\ M_\odot$) is acceptable, it is unlikely in terms of a mass range that can explode as an SN [$\lesssim 20\ M_\odot$; 8]. While the reason of the observed low N/O is not obvious, two possibilities are considered. One is the observational difficulty in distinguishing between the CSM and ejecta components in their X-ray spectra. Since these measurements were performed with RGS, it is technically hard to select only CSM regions that are expected to be in outermost shells. If the spectra is contaminated by ejecta emission and cannot be identified, it may result in an underestimate of the O abundance. Another possibility is an effect of binary evolution. Even in the case of a lower $M_{\rm ZAMS}$ progenitor ($\lesssim 15\ M_\odot$), the mass-loss rate is enhanced in a binary system and a lager contribution of O-rich winds from He-burning products significantly reduces N/O compared with the single star case [see also, 47]. This possibility is suggestively consistent with present binary population studies, in which high-mass X-ray binaries are more numerous in low-metallicity galaxies [59, 60]. It is required future follow-up investigations with larger sample of SNRs using a microcalorimeter onboard XRISM [24] and forthcoming missions such as Athena [25], Lynx [26], LEM [27], and HUBS [28].

5. Summary

Since stellar winds contain elements produced during stellar evolution, their abundance, especially those of C, N, and O reflect the progenitor properties. In SNRs, the wind-blown material is observed as surrounding shock-heated CSM, and therefore the detection of the CNO lines is crucial for obtaining direct information on their progenitors. Under this view, we calculated total amount of the CNO elements in the CSM using currently available stellar evolution codes. The result indicates that the abundance ratios of N/O and N/C are sensitive to the progenitor $M_{\rm ZAMS}$ and rotation velocities: these parameters can be a good probe to constrain the progenitor properties. A pilot study has been done by our previous observation [23] and another observation will be published soon [47]. While SNRs in which previous observations detected the C and N lines are still limited, we found that N is more overabundant than O (N/O $\sim$ 3) in most of galactic remnants whereas N/O is less than the solar abundance in those in the SMC and LMC except for SN 1987A. The reason for this discrepancy is still unclear though it may be attributed to the different metallicity environments. A more comprehensive systematic analysis will be required for many galactic/extra-galactic SNRs with the state-of-the-art instruments like *Resolve* on board XRISM.

A. Appendix

We here display the same plot as Figures 3, 4, and 5 in which N/C and N/O are converted to those of the mass ratios (Figures 6, 7, and 8).

Acknowledgments

The authors are very grateful to Takashi Yoshida, Jacco Vink, Satoru Katsuda, Hideyuki Umeda, Toshiki Sato, Kai Matsunaga, and Takaaki Tanaka for giving us precious advice on this

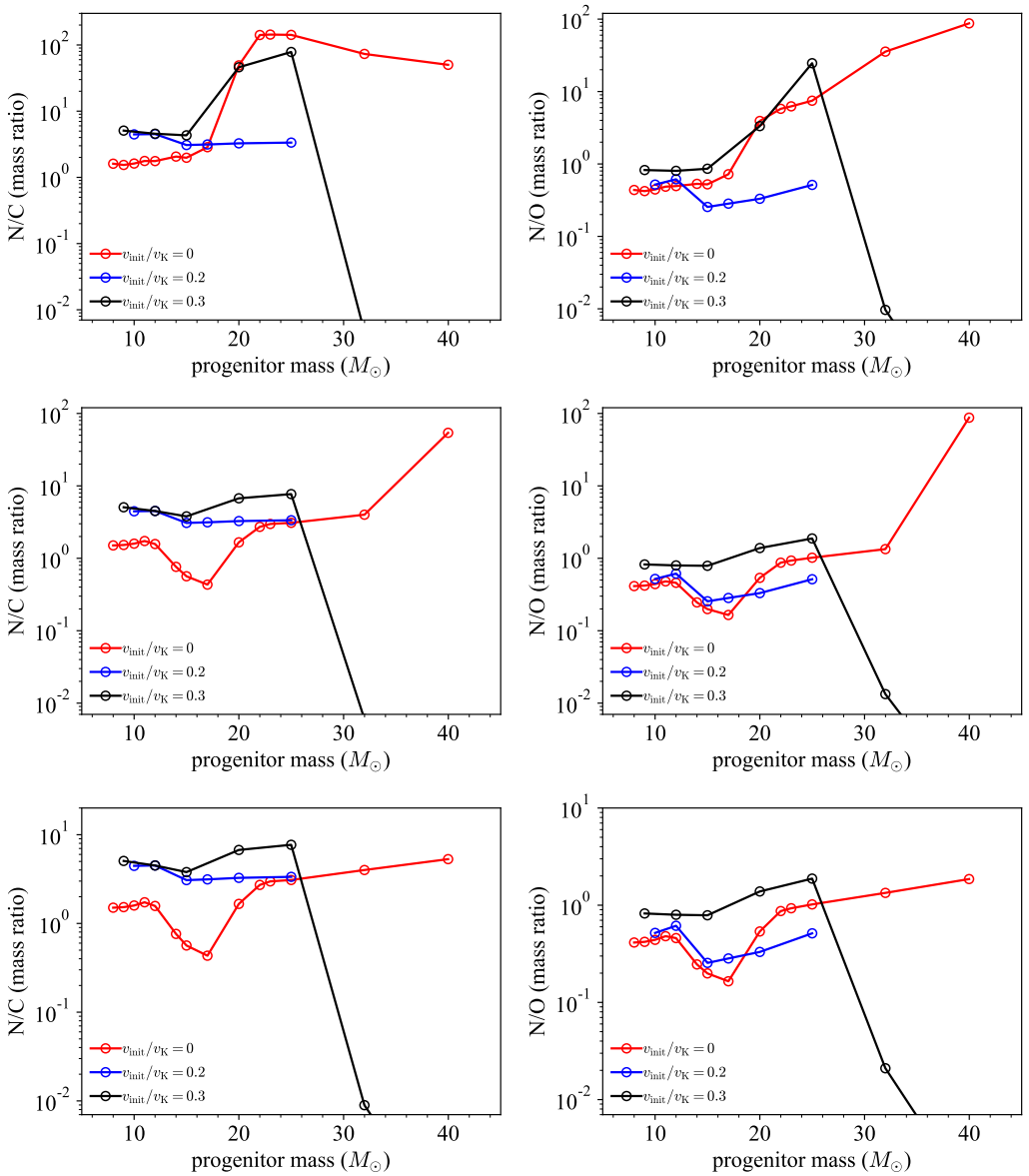

Figure 6: Same as Figure 3, but the x-axis is mass ratios.

study. This work is supported by JSPS Core-to-Core Program (grant number: JPJSCCA20220002) and JSPS/MEXT Science Research grant Nos. JP19K03915, JP22H01265 (H.U.), and JP23KJ1350 (T.N.).

References

[1] N. Smith, *Mass Loss: Its Effect on the Evolution and Fate of High-Mass Stars*, *ARA&A* **52** (2014) 487 [1402.1237].

[2] O. Yaron, D.A. Perley, A. Gal-Yam, J.H. Groh, A. Horesh, E.O. Ofek et al., *Confined dense*

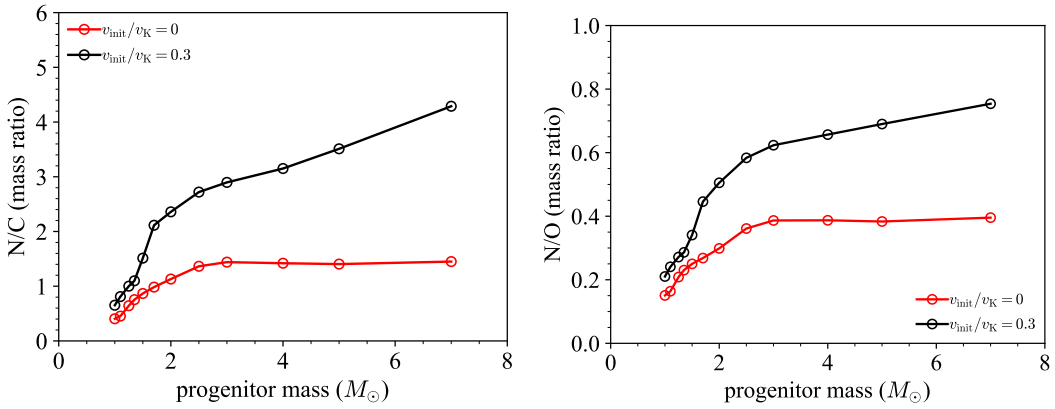

Figure 7: Same as Figure 4, but the x-axis is mass ratios.

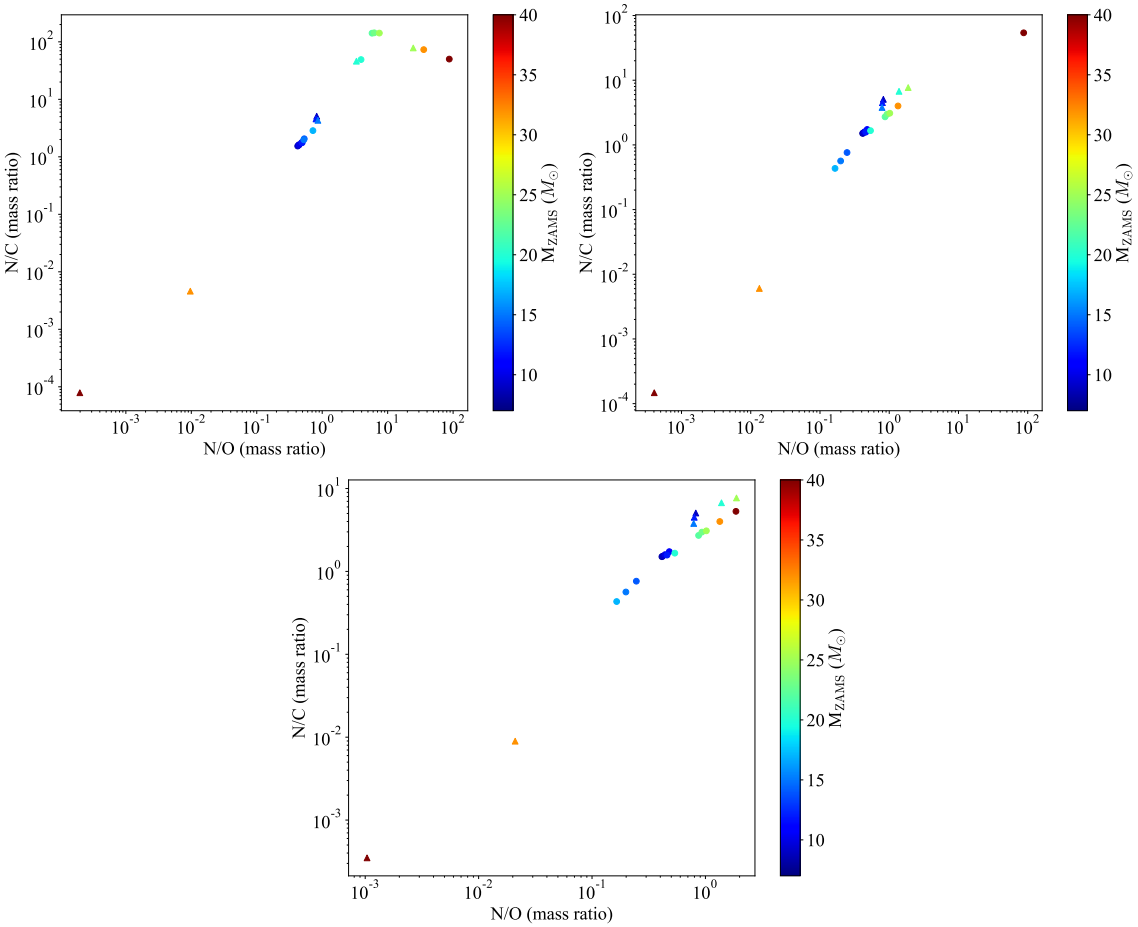

Figure 8: Same as Figure 5, but for mass ratios.

circumstellar material surrounding a regular type II supernova, *Nature Physics* **13** (2017) 510 [1701.02596].

[3] B. Dilday, D.A. Howell, S.B. Cenko, J.M. Silverman, P.E. Nugent, M. Sullivan et al., *PTF 11kx: A Type Ia Supernova with a Symbiotic Nova Progenitor*, *Science* **337** (2012) 942 [1207.1306].

[4] I. Hachisu, M. Kato and K. Nomoto, *A New Model for Progenitor Systems of Type IA Supernovae*, *ApJL* **470** (1996) L97.

[5] C. Badenes, J.P. Hughes, E. Bravo and N. Langer, *Are the Models for Type Ia Supernova Progenitors Consistent with the Properties of Supernova Remnants?*, *ApJ* **662** (2007) 472 [astro-ph/0703321].

[6] S.J. Smartt, *Progenitors of Core-Collapse Supernovae*, *ARA&A* **47** (2009) 63 [0908.0700].

[7] M. Díaz-Rodríguez, J.W. Murphy, D.A. Rubin, A.E. Dolphin, B.F. Williams and J.J. Dalcanton, *Progenitor Mass Distribution for Core-collapse Supernova Remnants in M31 and M33*, *ApJ* **861** (2018) 92 [1802.07870].

[8] T. Sukhbold, T. Ertl, S.E. Woosley, J.M. Brown and H.T. Janka, *Core-collapse Supernovae from 9 to 120 Solar Masses Based on Neutrino-powered Explosions*, *ApJ* **821** (2016) 38 [1510.04643].

[9] S. Katsuda, T. Takiwaki, N. Tominaga, T.J. Moriya and K. Nakamura, *Progenitor Mass Distribution of Core-collapse Supernova Remnants in Our Galaxy and Magellanic Clouds Based on Elemental Abundances*, *ApJ* **863** (2018) 127 [1807.03426].

[10] C. Fransson, P.M. Challis, R.A. Chevalier, A.V. Filippenko, R.P. Kirshner, C. Kozma et al., *Hubble Space Telescope and Ground-based Observations of SN 1993J and SN 1998S: CNO Processing in the Progenitors*, *ApJ* **622** (2005) 991 [astro-ph/0409439].

[11] A. Maeder, N. Przybilla, M.-F. Nieva, C. Georgy, G. Meynet, S. Ekström et al., *Evolution of surface CNO abundances in massive stars*, *A&A* **565** (2014) A39 [1404.1020].

[12] Y. Chiba, S. Katsuda, T. Yoshida, K. Takahashi and H. Umeda, *First detection of X-ray line emission from Type IIn supernova 1978K with XMM-Newton's RGS*, *PASJ* **72** (2020) 25 [2001.01975].

[13] S. Katsuda, K. Mori, K. Maeda, M. Tanaka, K. Koyama, H. Tsunemi et al., *Kepler's Supernova: An Overluminous Type Ia Event Interacting with a Massive Circumstellar Medium at a Very Late Phase*, *ApJ* **808** (2015) 49 [1506.03135].

[14] T. Kasuga, J. Vink, S. Katsuda, H. Uchida, A. Bamba, T. Sato et al., *Spatially Resolved RGS Analysis of Kepler's Supernova Remnant*, *ApJ* **915** (2021) 42 [2105.04235].

[15] H. Yamaguchi, F. Acero, C.-J. Li and Y.-H. Chu, *Discovery of Double-ring Structure in the Supernova Remnant N103B: Evidence for Bipolar Winds from a Type Ia Supernova Progenitor*, *ApJL* **910** (2021) L24 [2103.07599].

[16] B.T. Guest, W.P. Blair, K.J. Borkowski, P. Ghavamian, S.P. Hendrick, K.S. Long et al., *Locating the CSM Emission within the Type Ia Supernova Remnant N103B*, *ApJ* **926** (2022) 207 [2201.04653].

[17] J. Iben, I. and A.V. Tutukov, *Supernovae of type I as end products of the evolution of binaries with components of moderate initial mass.*, *Astrophysical Journal, Suppl. Ser.* **54** (1984) 335.

[18] R.F. Webbink, *Double white dwarfs as progenitors of R Coronae Borealis stars and type I supernovae.*, *The Astrophysical Journal* **277** (1984) 355.

[19] J. Whelan and J. Iben, Icko, *Binaries and Supernovae of Type I*, *ApJ* **186** (1973) 1007.

[20] S.P. Reynolds, K.J. Borkowski, U. Hwang, J.P. Hughes, C. Badenes, J.M. Laming et al., *A Deep Chandra Observation of Kepler's Supernova Remnant: A Type Ia Event with Circumstellar Interaction*, *ApJL* **668** (2007) L135 [0708.3858].

[21] E. Miyata, S. Katsuda, H. Tsunemi, J.P. Hughes, M. Kokubun and F.S. Porter, *Detection of Highly-Ionized Carbon and Nitrogen Emission Lines from the Cygnus Loop Supernova Remnant with the Suzaku Observatory*, *PASJ* **59** (2007) 163.

[22] H. Uchida, S. Katsuda, H. Tsunemi, K. Mori, L. Gu, R.S. Cumbee et al., *High Forbidden-to-resonance Line Ratio of O VII Discovered from the Cygnus Loop*, *ApJ* **871** (2019) 234 [1812.06616].

[23] T. Narita, H. Uchida, T. Yoshida, T. Tanaka and T.G. Tsuru, *Progenitor Constraint with Circumstellar Material for the Magnetar-hosting Supernova Remnant RCW 103*, *ApJ* **950** (2023) 137 [2304.11819].

[24] M. Tashiro, H. Maejima, K. Toda, R. Kelley, L. Reichenthal, J. Lobell et al., *Concept of the X-ray Astronomy Recovery Mission*, in *Space Telescopes and Instrumentation 2018: Ultraviolet to Gamma Ray*, J.-W.A. den Herder, S. Nikzad and K. Nakazawa, eds., vol. 10699 of *Society of Photo-Optical Instrumentation Engineers (SPIE) Conference Series*, p. 1069922, July, 2018, DOI.

[25] D. Barret, T. Lam Trong, J.-W. den Herder, L. Piro, M. Cappi, J. Houvelin et al., *The ATHENA X-ray Integral Field Unit (X-IFU)*, in *Space Telescopes and Instrumentation 2018: Ultraviolet to Gamma Ray*, J.-W.A. den Herder, S. Nikzad and K. Nakazawa, eds., vol. 10699 of *Society of Photo-Optical Instrumentation Engineers (SPIE) Conference Series*, p. 106991G, July, 2018, DOI [1807.06092].

[26] J.A. Gaskin, D.A. Swartz, A. Vikhlinin, F. Özel, K.E. Gelmis, J.W. Arenberg et al., *Lynx X-Ray Observatory: an overview*, *Journal of Astronomical Telescopes, Instruments, and Systems* **5** (2019) 021001.

[27] R. Kraft, M. Markevitch, C. Kilbourne, J.S. Adams, H. Akamatsu, M. Ayromlou et al., *Line Emission Mapper (LEM): Probing the physics of cosmic ecosystems*, *arXiv e-prints* (2022) arXiv:2211.09827 [2211.09827].

[28] J. Bregman, R. Cen, Y. Chen, W. Cui, T. Fang, F. Guo et al., *Scientific objectives of the Hot Universe Baryon Surveyor (HUBS) mission*, *Science China Physics, Mechanics, and Astronomy* **66** (2023) 299513 [2307.05672].

[29] K. Takahashi, T. Yoshida and H. Umeda, *Evolution of Progenitors for Electron Capture Supernovae*, *ApJ* **771** (2013) 28 [1302.6402].

[30] K. Takahashi, H. Umeda and T. Yoshida, *Stellar Yields of Rotating First Stars. I. Yields of Weak Supernovae and Abundances of Carbon-enhanced Hyper-metal-poor Stars*, *ApJ* **794** (2014) 40 [1406.5305].

[31] K. Takahashi, T. Yoshida and H. Umeda, *Stellar Yields of Rotating First Stars. II. Pair-instability Supernovae and Comparison with Observations*, *ApJ* **857** (2018) 111 [1803.06630].

[32] T. Yoshida, T. Takiwaki, K. Kotake, K. Takahashi, K. Nakamura and H. Umeda, *One-, Two-, and Three-dimensional Simulations of Oxygen-shell Burning Just before the Core Collapse of Massive Stars*, *ApJ* **881** (2019) 16 [1903.07811].

[33] S. Ekström, C. Georgy, P. Eggenberger, G. Meynet, N. Mowlavi, A. Wyttenbach et al., *Grids of stellar models with rotation. I. Models from 0.8 to 120 $M_\odot$ at solar metallicity ($Z = 0.014$)*, *A&A* **537** (2012) A146 [1110.5049].

[34] J. Wilms, A. Allen and R. McCray, *On the Absorption of X-Rays in the Interstellar Medium*, *ApJ* **542** (2000) 914 [astro-ph/0008425].

[35] R. Weaver, R. McCray, J. Castor, P. Shapiro and R. Moore, *Interstellar bubbles. II. Structure and evolution.*, *ApJ* **218** (1977) 377.

[36] R.A. Chevalier and J.N. Imamura, *Self-similar solutions for the interaction regions of colliding winds*, *ApJ* **270** (1983) 554.

[37] R.A. Chevalier, *Young Core-Collapse Supernova Remnants and Their Supernovae*, *ApJ* **619** (2005) 839 [astro-ph/0409013].

[38] S. Owocki, *Stellar wind mechanisms and instabilities*, in *EAS Publications Series*, M. Heydari-Malayeri, P. Stee and J.P. Zahn, eds., vol. 13 of *EAS Publications Series*, pp. 163–250, Jan., 2004, DOI.

[39] N. Przybilla, M. Firnstein, M.F. Nieva, G. Meynet and A. Maeder, *Mixing of CNO-cycled matter in massive stars*, *A&A* **517** (2010) A38 [1005.2278].

[40] N. Mauron and E. Josselin, *The mass-loss rates of red supergiants and the de Jager prescription*, *A&A* **526** (2011) A156 [1010.5369].

[41] L. Siess, *Evolution of massive AGB stars. III. the thermally pulsing super-AGB phase*, *A&A* **512** (2010) A10.

[42] A.I. Karakas and J.C. Lattanzio, *The Dawes Review 2: Nucleosynthesis and Stellar Yields of Low- and Intermediate-Mass Single Stars*, *PASA* **31** (2014) e030 [1405.0062].

[43] A. Heger, N. Langer and S.E. Woosley, *Presupernova Evolution of Rotating Massive Stars. I. Numerical Method and Evolution of the Internal Stellar Structure*, *ApJ* **528** (2000) 368 [astro-ph/9904132].

[44] B.F. Williams, T.J. Hillis, J.W. Murphy, K. Gilbert, J.J. Dalcanton and A.E. Dolphin, *Constraints for the Progenitor Masses of Historic Core-collapse Supernovae*, *ApJ* **860** (2018) 39 [1803.08112].

[45] S.C. Yoon, S.E. Woosley and N. Langer, *Type Ib/c Supernovae in Binary Systems. I. Evolution and Properties of the Progenitor Stars*, *ApJ* **725** (2010) 940 [1004.0843].

[46] S.-C. Yoon, *Towards a better understanding of the evolution of Wolf-Rayet stars and Type Ib/Ic supernova progenitors*, *MNRAS* **470** (2017) 3970 [1706.04716].

[47] T. Narita, H. Uchida, J. Vink, H. Umeda, T. Yoshida, T. Sato et al., *Oxygen-rich circumstellar material from stripped envelope produced in binary system detected in supernova remnant G292.0+1.8*, *in prep.* .

[48] T. Tanaka, T. Okuno, H. Uchida, H. Yamaguchi, S.-H. Lee, K. Maeda et al., *Rapid Deceleration of Blast Waves Witnessed in Tycho's Supernova Remnant*, *ApJL* **906** (2021) L3 [2012.13622].

[49] Y. Tanaka, H. Uchida, T. Tanaka, Y. Amano, Y. Koshiba, T. Go Tsuru et al., *Charge Exchange X-Ray Emission Detected in Multiple Shells of Supernova Remnant G296.1-0.5*, *ApJ* **933** (2022) 101 [2205.10038].

[50] P. Lundqvist and C. Fransson, *The Line Emission from the Circumstellar Gas around SN 1987A*, *ApJ* **464** (1996) 924 [astro-ph/9512025].

[51] L. Sun, J. Vink, Y. Chen, P. Zhou, D. Prokhorov, G. Pühlhofer et al., *The Post-impact Evolution of the X-Ray-emitting Gas in SNR 1987A as Viewed by XMM-Newton*, *ApJ* **916** (2021) 41 [2103.03844].

[52] H. Suzuki, H. Yamaguchi, M. Ishida, H. Uchida, P.P. Plucinsky, A.R. Foster et al., *Plasma Diagnostics of the Supernova Remnant N132D using Deep XMM-Newton Observations with the Reflection Grating Spectrometer*, *ApJ* **900** (2020) 39 [2007.06158].

[53] K.J. van der Heyden, J.A.M. Bleeker, J.S. Kaastra and J. Vink, *High resolution spectroscopy and emission line imaging of DEM L 71 with XMM-Newton*, *A&A* **406** (2003) 141 [astro-ph/0305103].

[54] S. Broersen, J. Vink, J. Kaastra and J. Raymond, *The high resolution X-ray spectrum of SNR 0506-68 using XMM-Newton*, *A&A* **535** (2011) A11 [1109.1560].

[55] Y. Koshiba, H. Uchida, T. Tanaka, Y. Amano, H. Sano and T.G. Tsuru, *High-resolution X-ray study of supernova remnant J0453.6-6829 with unusually high forbidden-to-resonance ratio*, *PASJ* **74** (2022) 757 [2204.09364].

[56] K.A. Frank, D.N. Burrows and S. Park, *Chandra Observations of SNR RCW 103*, *ApJ* **810** (2015) 113 [1508.01513].

[57] P. Lundqvist and C. Fransson, *Circumstellar Emission from SN 1987A*, *ApJ* **380** (1991) 575.

[58] C.J. Burrows, J. Krist, J.J. Hester, R. Sahai, J.T. Trauger, K.R. Stapelfeldt et al., *Hubble Space Telescope Observations of the SN 1987A Triple Ring Nebula*, *ApJ* **452** (1995) 680.

[59] L.M. Dray, *On the metallicity dependence of high-mass X-ray binaries*, *MNRAS* **370** (2006) 2079 [astro-ph/0606200].

[60] V.M. Douna, L.J. Pellizza, I.F. Mirabel and S.E. Pedrosa, *Metallicity dependence of high-mass X-ray binary populations*, *A&A* **579** (2015) A44 [1505.05483].

COMMENT

FRANCO GIOVANNELLI: There is a paper by Bernd Aschenbach (2016), in which he reconsidered Sedov's formula for the age of SNRs. I suggest you to read this paper that probably can help you in your considerations.

HIROYUKI UCHIDA: I read this paper with great interest. The author claim that an energy transfer to cosmic ray acceleration will impact on the dynamical evolution of SNRs and particularly the age estimates. Our method depends on the SNR radius, which can be independently determined by the SNR distance.

PoS(MULTIF2023)044